An analytical approach to calculate stress concentration factors of machined surfaces

I. Perez [(1)], A. Madariaga [*(1)], P.J. Arrazola [(1)], M. Cuesta [(1)], D. Soriano [(1)]

[1]Mechanical and Industrial Production Department, Faculty of Engineering, Mondragon Unibertsitatea, Spain

Corresponding author:

Aitor Madariaga, Mechanical and Industrial Production Department, Faculty of Engineering, Mondragon Unibertsitatea, Loramendi 4, 20500 Mondragon, Spain.

E-mail address: amadariaga@mondragon.edu

Abstract

Machining operations affect the properties of the final surface layer, and these can impact on its functional performance, particularly on fatigue behaviour. Among the properties of the machined surface, surface topography is one major parameter affecting fatigue behaviour. The literature review has demonstrated that stress concentration factors K_t of the surface provide a more reliable estimation of the impact on the fatigue behaviour of machined components. Finite Element (FE) simulations can accurately calculate the stress concentration factor of machined surfaces, but they incur a high computational cost. Recent advances have shown that analytical models can reliably determine stress concentration factors of 2D roughness profiles. However, analytical models that predict stress concentration factors of 3D surface topographies are still lacking. This paper is aimed at developing an analytical method to calculate the stress concentration factor K_t of 3D surfaces generated by machining operations. To validate the model, a specimen of 7475-T7351 aluminium alloy was face milled and its surface topography was characterised using an Alicona IFG4 profilometer. Stress concentration factors were calculated in the selected surface regions using the proposed analytical model, and later compared to results obtained by FE simulations. The mean difference in the stress concentration factor K_t calculated by the proposed analytical and FE models is of 1.53%. Importantly, the developed analytical model reduces the computing time by 3000 times compared to FE models, and enables the analysis of larger surfaces.

Keywords

Surface topography, stress concentration factor, fatigue, modelling

1. Introduction

The processes applied in the last stage of the manufacturing route of a component, such as machining operations, can significantly affect the properties of the surface layer. These properties define the Surface Integrity (SI) of the component and include surface topography and subsurface properties (residual stresses, microhardness variations or microstructural defects). It is well known that SI plays a major role in the functional performance of components subjected to cyclical loadings [1-5], particularly in fatigue behaviour since cracks generally initiate from free surfaces [5]. Therefore, it is necessary to fulfil SI requirements so as to prevent early fatigue failures of components such as moulds, gears, bearings and shafts. Such failures can have a detrimental effect on operating costs [5]. This is even more important when producing critical components, such as aeroengine parts, where poor SI can endanger the safety of passengers.

Historically, empirical correction factors that modify fatigue endurance have been used to quantify the effect of manufacturing processes (i.e. machining, polishing or forging) on fatigue behaviour [6,7]. The surface properties of a component are very sensitive to the manufacturing conditions and consequently, this implies performing a specific fatigue behaviour characterisation for each manufacturing condition, to determine reliable empirical correction factors. However, it is widely accepted that the SI of the component significantly affects fatigue life.

Many authors have studied the effect of SI on the fatigue behaviour of machined surfaces. Although these efforts have enabled understanding the effect of machining conditions on the SI of machined components, the correlation between SI and in-service fatigue behaviour is not yet widely understood. It is generally accepted that surface

anomalies generated during machining are detrimental to fatigue life of components. Some authors [8-11] have found that cracks, carbide/particle break outs, severe plastic deformation, material drag, or white layers produced by different machining processes reduce the fatigue strength of specimens. Other researchers have shown that the effect of residual stresses on fatigue performance can be significant, especially in the absence of microstructural damage and/or when roughness is low [12-19]. On the other hand, some authors have observed that higher surface roughness reduces fatigue strength, and this reduction is significant when surface residual stresses are negligible or are relaxed during cyclic loading [9, 20-24]. However, these findings are frequently limited to the range of tested conditions. It is therefore much more effective to analyse, understand and quantitatively determine the effect of each SI parameter on fatigue life. This knowledge would definitively contribute to the development of more accurate models to estimate the fatigue life of components.

This paper has a particular focus on the effect of surface topography on the fatigue performance of machined components, since it is one major parameter of SI affecting fatigue behaviour. In fact, Novovic *et al.* [5] concluded that average surface roughness values higher than R_a = 0.1 μm heavily influence the fatigue performance of machined components if residual stresses are negligible. Traditionally, average roughness R_a has been used to analyse the effect of surface roughness on fatigue behaviour. However, a reliable quantitative relationship between 2D surface roughness descriptors and fatigue behaviour has not yet been established.

Recent developments in areal topography measurement deliver the fast acquisition of high-density surface datasets, allowing the reconstruction of detailed 3D digital models of surface topography [25]. These advances also enable further analysis

of the effect of 3D surface parameters on fatigue performance. For instance, some authors [26, 27] suggest that areal topography parameters such as S_a, S_p, S_v (the arithmetical average height, maximum peak height, maximum pit height and maximum height of the scale-limited surface) show a greater correlation with fatigue performance than traditional 2D roughness parameters. Some researchers have also found good agreement between multi-scale curvature parameters and the fatigue limit of milled specimens [28]. However, it should be noted that if two surfaces have the same value of the principal index S_a, their surface micro geometrical features can differ significantly leading to completely distinct performance properties [29]. Therefore, it is insufficient to rely on only one or several single-value principal surface topography parameters when assessing the functionality of the surface.

Fundamentally, the micro-geometrical irregularities that constitute surface roughness/topography can be studied as microscopic notches, which act as stress riser that can promote fatigue crack initiation [22, 30]. Interestingly, based on this concept, some other researchers have quantified the effect of surface roughness/topography generated by machining in terms of the stress concentration factor (K_t), considering that its effect is similar to a notch effect [22-24, 27].

Some authors have developed semi-empirical models to determine the stress concentration factor of machined surfaces as a function of arithmetic surface parameters. Based on the expression developed by Peterson [31] of K_t for a single notch, Neuber [32] proposed an expression for the stress concentration factor induced by roughness, considered as a series of succeeding notches. Later, several authors further developed this expression of K_t adding more parameters that describe the surface roughness, such as R_a, R_y, R_z and R_q [33-37]. More recently, and taking into account the

limitations of 2D parameters of surface profiles, some other authors have developed new K_t expressions using 3D special parameters of the surface topography such as S_a, S_y, S_z and S_q [27, 37]. The stress concentration factor is obtained assuming the roughness as a series of successive notches. Nevertheless, arithmetic correlation is not accurate enough as does not consider local defects/topology of the topography and it calculates the mean value of the K_t instead of the critical value.

Alternatively, some other researchers have calculated the stress concentration factors of machined surfaces using Finite Element (FE) models [22-24, 38-41]. The modelling procedure consist of: i) importing the geometry of the measured surface, ii) applying a uniform load in the direction of interest, and iii) analysing the ratio between the resulting stress at each point and the applied stress to quantify K_t. As these FE models are based on the geometry of the real surface, they can also describe local effects and are more reliable than the previous models described by means of arithmetic parameters. Based on the results of FE models, Abroug *et al.* [24, 39] and Li *et al.* [40] stated that the S_a roughness parameter is directly related to K_t. However, Ardi *et al.* [41] found a considerable scatter on the relationship between the height of the surface and the specific K_t of each point. Once again, these contradictions highlight the difficulty of quantifying the effect of surface measurement descriptors on K_t, and consequently on fatigue behaviour.

FE models provide accurate estimations of the stress concentration factor, but they incur a high computational cost and calculus time. To overcome this drawback, recent research has focused on the development of analytical expressions of K_t that take into account the roughness profile and not only the arithmetic values of it. In 2016, Medina [42] developed the first fully analytical model to calculate stress concentration

factors for a wide range of shallow undulating surfaces, which was based on a previous work done by Gao [43]. Later, Cheng *et al*. [44] and Ma *et al*. [45] applied Medina's approach to determine the stress concentration factor of 2D roughness profiles generated by machining. They defined the surface roughness profile using the Fourier series and obtained the expression of K_t performing a first order perturbation analysis. Both studies showed good agreement between the results obtained by the analytical method and calculations done by FE simulations. For instance, Ma *et al*. [45] reported relative errors below 8% in their case-study.

Recently, Kantzos *et al*. [46] developed a Convolutional Neural Network (CNN) to determine the K_t for a 3D surface topography without high computational cost. The neural network was trained from results obtained from an Elasto-Viscoplastic Fast Fourier Transform-based mechanical model [47]. This model discretizes the surface on infinitesimal microstructures and calculates the response to an applied strain. The CNN does not imply a high computational cost, but it needs to be trained with lots of surfaces. Furthermore, it is not a robust model as it has no physical foundation.

The literature review has demonstrated that the sole use of surface measurement descriptors is not enough to quantify the effect of surface topography on the fatigue behaviour of machined components. The determination of stress concentration factors K_t of machined surfaces provides a more reliable estimation of the impact on their fatigue behaviour. FE simulations can accurately determine the stress concentration factor of machined surfaces, but they incur a high computational cost and can only analyse small surfaces. Recent advances have shown that analytical models can reliably determine stress concentration factors of 2D roughness profiles. However, physics based analytical models that predict stress concentration factors of 3D surface

topographies are still lacking in the literature. These models are necessary to map stress concentration factors of machined surfaces with 3D features, for example, those produced by milling operations. Interestingly, the development of these analytical models can definitely contribute to a fast estimation of stress concentration factors of 3D surfaces reducing the use of specialized and time-consuming FEM software.

This paper is aimed at developing an analytical method to map the stress concentration factor K_t of 3D surfaces generated by machining operations. First, the analytical model used to calculate stress concentration factors of 2D roughness profiles is briefly described. Then, the method is further developed to map stress concentration factors of 3D surface topographies in two different loading directions. To validate the model, a specimen of 7475-T7351 aluminium alloy was face milled and its surface topography was characterised using an Alicona IFG4 profilometer. Stress concentration factors were calculated in the selected surface regions (regions with characteristic features) using the developed analytical model, and later compared to results obtained by FE simulations for the same surface regions. Finally, the differences between FE and the developed analytical model are discussed, as well as the recommendations to apply the developed methodology.

2. Theory

2.1. Background: stress concentration factors of 2D roughness profiles

The surface topography of a machined surface can be studied as a random process that does not change over time (stationary stochastic process) and it can be calculated by superposing a series of sinusoidal components through spectrum analysis as suggested by Aono and Noguchi [48] (see Figure 1). Essentially, Fourier

Transformation converts spatial information into spectral information, and enables the assessment of the frequency content of the profile or surface [49]. By these means, the surface topography $z(x)$ is defined as a Fourier series by a given n number of cosines and sinuses with a_i and b_i amplitudes and f_i frequency, as shown in eq. 1.

$$z(x) = \sum_{i=1}^{n} a_i \cdot \cos(2\pi \cdot f_i \cdot x) + b_i \cdot \sin(2\pi \cdot f_i \cdot x) \quad \text{(eq.1)}$$

assuming $\sqrt{{a_i}^2 + {b_i}^2} \cdot f_i \ll 1$ (eq.2)

a) b)

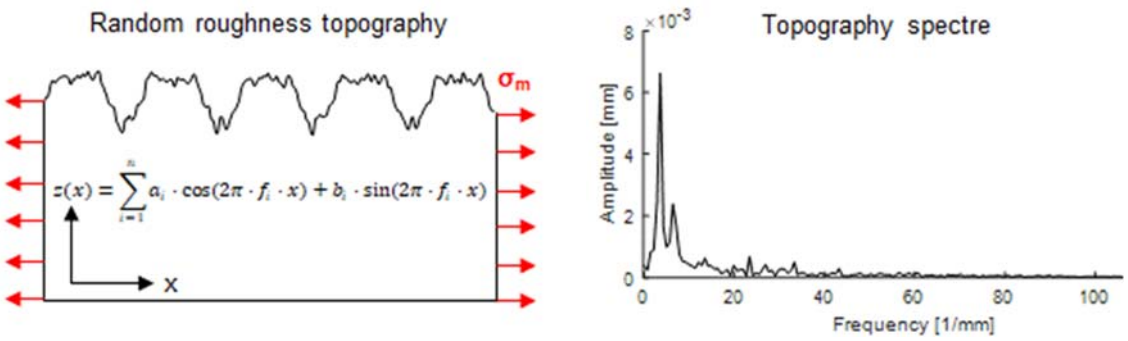

Figure 1. a) Example of a random roughness profile subjected to a uniform longitudinal load σ_m, and b) spectral information of the profile obtained by the Fourier Transformation

Considering the topography as a shallow surface eq.2 that is subjected to plane stress conditions, the stress concentration factor can be obtained by performing a first order perturbation analysis [44, 45]. Applying a uniform longitudinal stress σ_m to the surface layer (see Figure 1) and performing a first order perturbation analysis, the local stress σ_{xx} is represented by the expression shown in eq.3. Finally, the stress

concentration factor K_{txx} is defined in eq.4, as the ratio between the local stress state σ_{xx} and the applied stress σ_m.

$$\sigma_{xx}(x) = \sigma_m + 4\pi\sigma_m \cdot \left(\sum_{i=1}^{n} a_i \cdot f_i \cdot \cos(2\pi \cdot f_i \cdot x) + b_i \cdot f_i \cdot \sin(2\pi \cdot f_i \cdot x) \right) \quad \text{(eq.3)}$$

$$K_{t_{xx}}(x) = \frac{\sigma_{xx}}{\sigma_m} = 1 + 4\pi \cdot \left(\sum_{i=1}^{n} a_i \cdot f_i \cdot \cos(2\pi \cdot f_i \cdot x) + b_i \cdot f_i \cdot \sin(2\pi \cdot f_i \cdot x) \right) \quad \text{(eq.4)}$$

2.2. Methodology to calculate stress concentration factors of 3D topographies

The first order perturbation analysis used for obtaining the stress concentration factor of 2D shallow profiles can only be applied under plane stress state conditions. To extend the methodology and calculate stress concentration factors of 3D surface topographies subjected to constant stress (normal stresses or bending stresses) the following hypothesis is assumed in this method: if the measured surface has a good resolution, the difference in the roughness height Δz (x, y) between adjacent 2D profiles is minimal, and consequently the difference in the stress state will also be minimal. Therefore, if the topography is divided into 2D profiles, first order perturbation analysis can be applied to each segment. This hypothesis is validated in Section 4.

The first step to calculate the K_t of a 3D surface topography consists of dividing the topography into 2D segments, as shown in Figure 2. The topography is formed by a total of n points with x, y and z position vectors. In this step the roughness height vector z is transformed into a matrix of $i \times j \approx n$ size, where each column corresponds to a given x position and each row to a y position (eq.5). Therefore, each row represents data of a 2D roughness profile of each y_j point position, and consequently eq. 4 can be applied to determine the K_{txx} of each 2D profile. When the first order perturbation analysis is

applied in all *y* segments, the general expression shown in eq.6 is obtained. The number of Fourier series or frequencies used in each *y* segment is limited to *j*/2 to fulfil Nyquist theorem [50, 51]. If this criterion is not met, an aliasing could appear on the calculated stress concentration map, which would not correspond to the measured topography.

$$\{z\}_{1\times n} \longrightarrow [z]_{i\times j} = \begin{bmatrix} z_{11}(x_1, y_1) & z_{12}(x_2, y_1) & \dots & z_{1j}(x_j, y_1) \\ z_{21}(x_1, y_2) & z_{22}(x_2, y_2) & \dots & z_{2j}(x_j, y_2) \\ \dots & \dots & \dots & \dots \\ z_{i1}(x_1, y_i) & z_{i2}(x_2, y_i) & \dots & z_{ij}(x_j, y_i) \end{bmatrix} \quad \text{(eq.5)}$$

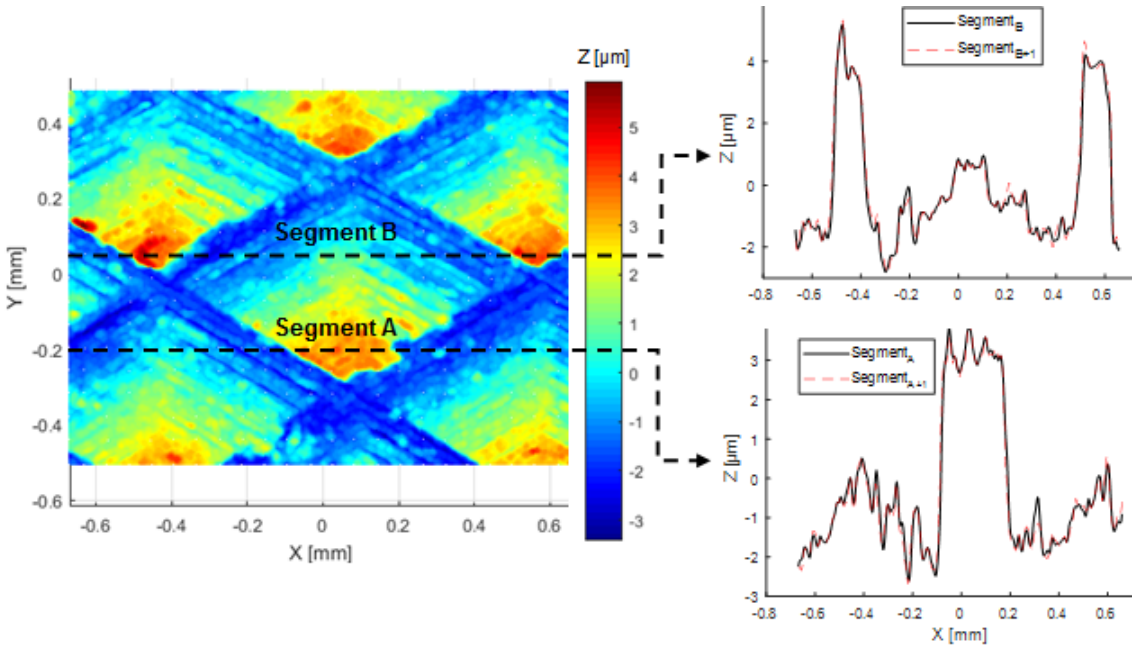

Figure 2. Example of a 3D surface topography *z*(*x*,*y*) measured using an optical profilometer (left) and, 2D profiles *z*(*x*) of segments A and B of the measured surface.

$$\{K_{t_{xx}}(x)\}_{i\times 1} = 1 - 4\pi \left\{ \begin{array}{l} \sum_{k=1}^{j/2} f_{1k} \cdot (a_{1k}\cos(2\pi f_{1k} \cdot x) + b_{1k}\sin(2\pi f_{1k} \cdot x)) \\ \sum_{k=1}^{j/2} f_{2k} \cdot (a_{2k}\cos(2\pi f_{2k} \cdot x) + b_{2k}\sin(2\pi f_{2k} \cdot x)) \\ \dots \\ \sum_{k=1}^{j/2} f_{ik} \cdot (a_{ik}\cos(2\pi f_{ik} \cdot x) + b_{jk}\sin(2\pi f_{ik} \cdot x)) \end{array} \right\} \quad \text{(eq.6)}$$

Importantly, the proposed methodology enables the calculation of the stress concentration factor of 3D surface topography when the stress is applied in both the *x* and *y* direction. This is an interesting outcome for multiaxial loading states. The steps explained in the preceding paragraph are still valid to determine the stress concentration factor K_{tyy} in the *y* direction. If the *z* matrix is transposed, a *j*×*i* sized matrix can be obtained, where each row represents the 2D profile of each *x* point (eq.7). Finally, applying eq.4 in the *y* direction, the general expression of K_{tyy} is obtained in eq.8.

$$[z]_{i\times j} \longrightarrow [z]^{\mathrm{T}}{}_{j\times i} = \begin{bmatrix} z_{11}(x_1, y_1) & z_{12}(x_1, y_2) & \dots & z_{1i}(x_1, y_i) \\ z_{21}(x_2, y_1) & z_{22}(x_2, y_2) & \dots & z_{2i}(x_2, y_i) \\ \dots & \dots & \dots & \dots \\ z_{j1}(x_j, y_1) & z_{j2}(x_j, y_2) & \dots & z_{ji}(x_j, y_i) \end{bmatrix} \quad \text{(eq.7)}$$

$$\left\{K_{t_{yy}}(y)\right\}_{j\times 1} = 1 - 4\pi \left\{ \begin{array}{c} \sum_{k=1}^{i/2} f_{1k} \cdot (a_{1k}\cos(2\pi f_{1k} \cdot y) + b_{1k}\sin(2\pi f_{1k} \cdot y)) \\ \sum_{k=1}^{i/2} f_{2k} \cdot (a_{2k}\cos(2\pi f_{2k} \cdot y) + b_{2k}\sin(2\pi f_{2k} \cdot y)) \\ \dots \\ \sum_{k=1}^{i/2} f_{jk} \cdot \left(a_{jk}\cos\left(2\pi f_{jk} \cdot y\right) + b_{jk}\sin\left(2\pi f_{jk} \cdot y\right)\right) \end{array} \right\} \quad \text{(eq.8)}$$

3. Materials and methods

3.1. Machining experiment

The specimen for the machining test was extracted by water jet assisted machining from a 40 mm thick 7475-T7351 aluminium rolled plate, obtaining a specimen of dimensions 100×80×40 mm. The clamping of the specimen and strategy followed during the face milling of the upper side of the specimen is shown in Figure 3.

The tool path was not centred along the width so as to obtain significantly different topographies in the transverse direction.

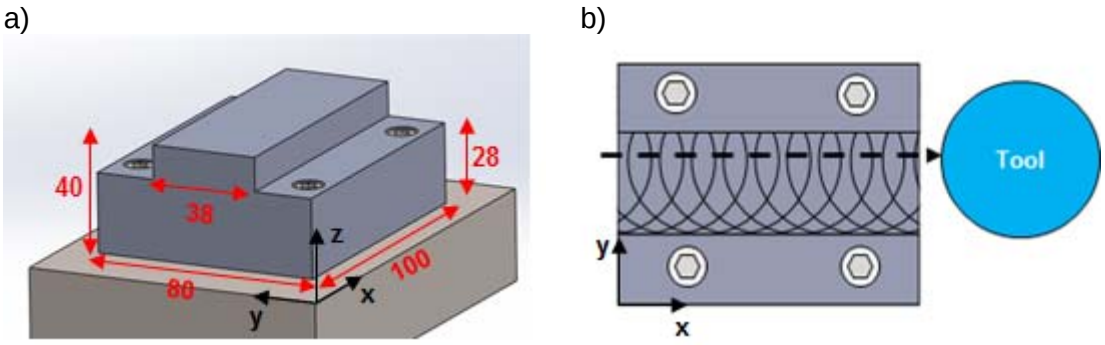

Figure 3. a) Geometry and dimensions (in mm) of the specimen used in the face milling experiment, and b) schematic representation of the tool path (upper view) during the face milling

First, the specimen was face milled under roughing conditions. Then, the finishing up-milling operation was carried out in the cutting conditions summarised in Table 1. An indexable face milling cutter with a diameter of 50 mm and five uncoated inserts (APKT L93 1604PDFR) was used in the face milling test. The properties of the inserts are shown in Table 2.

Table 1. Cutting conditions of the machined specimen

Cutting speed [m/min]	Feed rate [mm/tooth]	Depth of cut [mm]	Width of cut [mm]
800	0.20	1	37.5

Table 2. Properties of the APKT L93 1604PDFR uncoated inserts.

Material	Rake angle [º]	Clearance angle [º]	Nose radius [mm]	Edge radius [µm]
Uncoated WC-Co	11	8	0.2	12-18

3.2. Surface characterisation

Three regions (with different features) of the machined surface of the specimen were characterised to validate the proposed methodology and the hypothesis. Figure 4

shows the face milled surface and identifies the three small topographic regions that were analysed in greater detail: *EdgeShort* (0.9×1.15 mm), *EdgeLong* (1.25×3.2 mm) and *CentreWide* (3×2 mm).

The surface topography of the selected regions was measured using an Alicona IFG4 optical profilometer with a 20× magnifying objective lens. Table 3 shows the parameters used in the set-up, including both vertical and horizontal resolutions. The light source was set between 0.08-0.12 out of 1, and the polarizer of the profilometer was deactivated during the measurements so that the surface was visible.

Table 3. Main parameters defined for the measurements of surface topographies in the Alicona IFG4 profilometer.

Objective	Horizontal resolution	Vertical resolution	Light source	Polarizer
20×	5 µm	50 nm	0.8-0.12	No

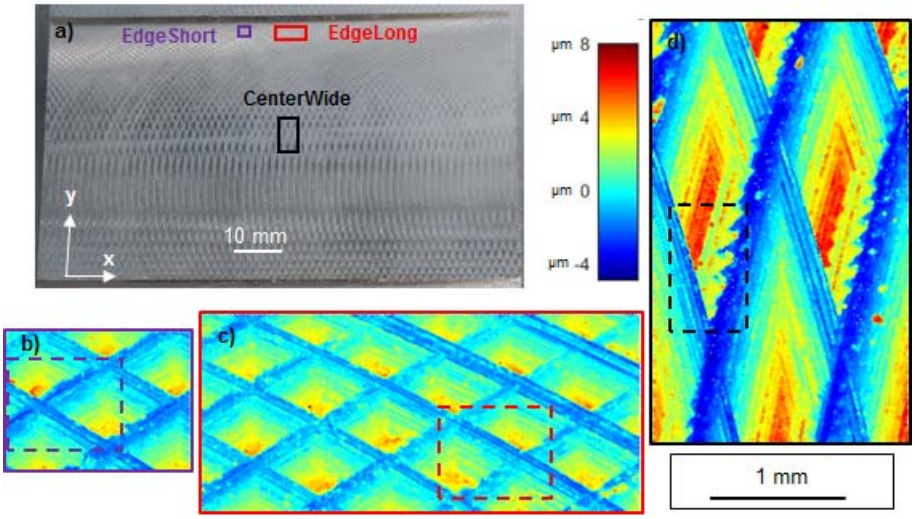

Figure 4. a) Image of the face milled surface showing the location of the surfaces measured using an optical profilometer, and plots of the measured surface topographies: b) *EdgeShort* c) *EdgeLong*, d) *CentreWide*.

3.3. FE model

To validate the analytical methodology proposed in section 2.2. the stress concentration factors of the three selected regions were also calculated using an FE model. It should be noted that this analysis was performed in a reduced area of 0.5 mm^2 of each of the selected regions (see dashed lines in Figure 4) to overcome the high computational cost of accurate FE models.

The first step of the FE model is creating the geometry to be analysed. As the measured topographic regions were formed by a point cloud, these were initially transformed into a 3D surface geometry. Then, a solid block was extruded from the generated surfaces, creating the 3D solid parts that were analysed in Abaqus software. These solid parts were modelled as solid homogeneous aluminium with a Young modulus of 71 GPa and a Poisson's ratio of 0.33. It should be clarified that the stress concentration factors depend on geometry and material properties are not critical in this FE model.

To determine the distribution of the stress concentration factor K_{txx}, a tensile stress of σ_m=1 MPa was applied in the x direction to one face, constraining the x displacement on the opposite face (see Figure 5.a). Then, σ_{xx} stresses were measured in the x direction, and $K_{txx}= \sigma_{xx}/ \sigma_m$ was calculated. The same procedure was used to obtain the stress concentration factor K_{tyy}: a tensile stress of σ_m=1 MPa was applied in the y direction to one face, constraining the y displacement on the opposite face (see Figure 5.b). Finally, σ_{yy} stresses were measured in the y direction, and $K_{tyy}= \sigma_{yy}/ \sigma_m$ was determined.

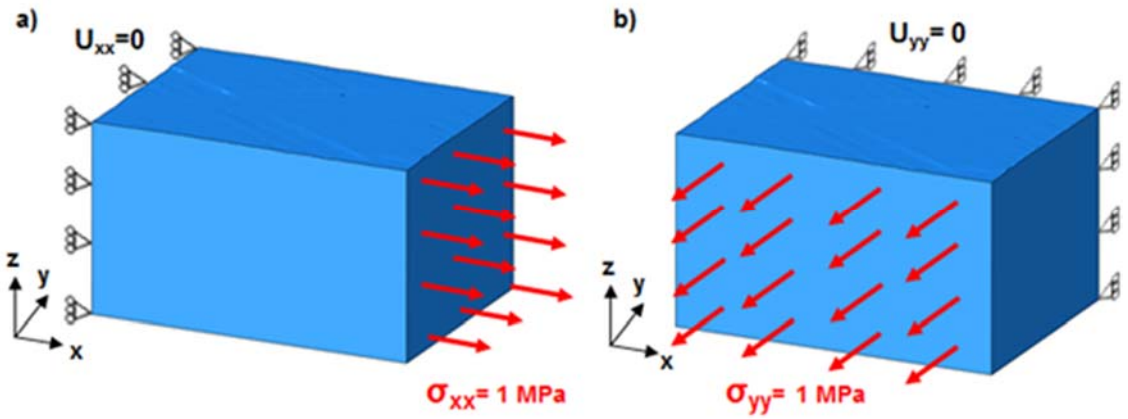

Figure 5. Boundary and loading cases of the FE model to obtain the stress concentration factor K_t a) in *x* direction (unitary stress in *x* and constrained *x* displacement on the opposite face) and b) in *y* direction (unitary stress in *y* and constrained *y* displacement on the opposite face)

The parts were meshed using C3D10 type tetrahedral elements, due to the complexity of the geometry of the surface topographies. The nodal distance of the elements ranged from 3 to 25 µm, locating the lower size elements near the surface and increasing the size beneath the surface. The lowest element size of 3 µm located near the surface was defined after setting the horizontal resolution of the measured topography. For example, to analyse the topographic region labelled *EdgeShort*, 640,000 elements were defined in the surface layer of the part, while 490,000 elements were defined in the remaining solid. With this meshing strategy, more than 1 million C3D10 elements were used to calculate the K_t of each analysed surface.

4. Results

Figure 6 shows the stress concentration factor K_t obtained with both analytical and FE models for the topographic region *EdgeLong* when the stress was applied to the transversal *y* direction. The highest stress concentrations (mean value of 1.6) are located

in the valleys of the topography, as can be seen in Figure 6.a. The maximum stress concentrations are not located in the deepest valleys, but in the highest change of height (valley to peak) along the analysed direction. It should be noted that values of K_t greater than 10 were calculated on the edges of the topography along the analysed *y* direction. However, this was produced due to a boundary effect in the borders of the analytical model, as it is assumed to be a semi-infinite plate with a repeating profile [35]. Therefore, the results obtained on the edges should not be included in the post-analysis.

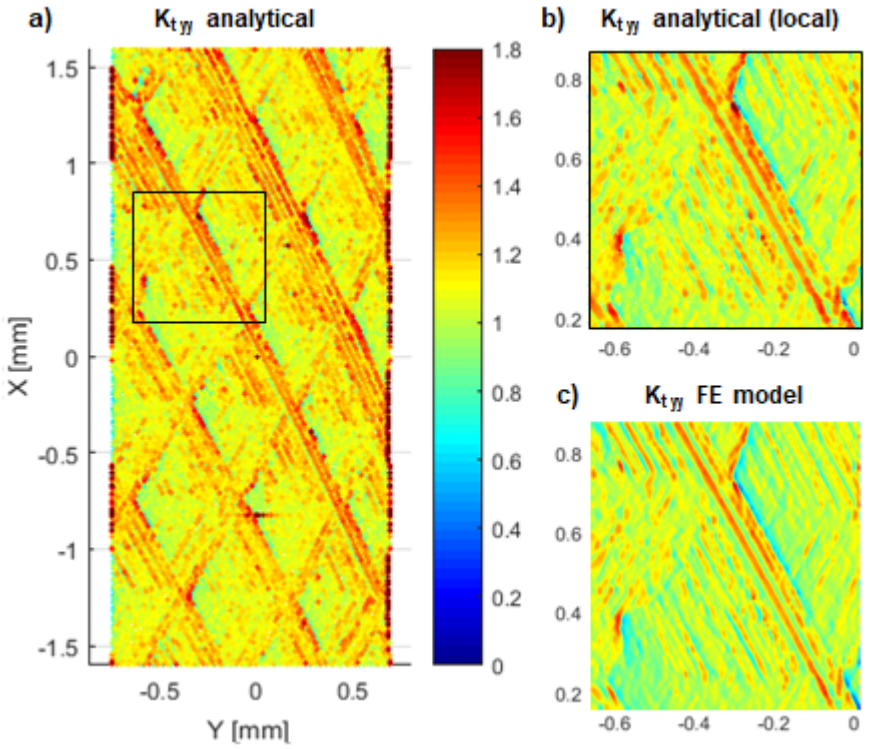

Figure 6. Stress concentration factor K_t of surface *EdgeLong* (stresses in *y* direction): a) analytical results of the entire surface and location of the reduced area for a detailed analysis, b) analytical results of the reduced area and c) comparison with the FE model in the reduced area.

Figure 6.b compares the results obtained by the analytical model and FE model when calculating the stress concentration factor K_t in the *y* direction of the *EdgeLong* surface. The results of the stress concentration factors obtained with the FE and

analytical models in the reduced area show good agreement, with a mean deviation of 4.8%. This deviation increases at the valleys of the topography. The highest deviation is of 11.5% and is located at the highest value of the K_t (1.81 for the analytic model and 1.62 for the FE model). Therefore, these results confirm that the hypothesis stated in section 2.2. is valid for the calculation of stress concentration factors of 3D surface topographies.

The same analysis was carried out for the two other selected topographies in both the *x* and *y* directions. The trend was almost identical between the analytical and FE models, with a small deviation that also increased in the valleys. Figure 7 compares the maximum values of K_t calculated with the analytical and FE models for the analysed cases at the same point. The bar called "Analytical local" corresponds to the value obtained with the analytical model located at the same point as the maximum value of K_t of the FE model. The highest value of K_t is located in the region *CenterWide* (maximum value of 1.86 in the FE model and 1.94 in the analytical model), when it was loaded in the *y* direction. Furthermore, *CenterWide* showed a similar value of maximum K_t when the stress was applied in both the *x* and *y* direction.

The differences observed between the FE and analytical models are low, ranging from 2.8% to 11.54% (see Figure 7). The highest difference appeared in the *EdgeLong* surface when it was loaded in the *y* direction. It should be noted that for some surfaces, such as *EdgeShort* in the *x* direction, the critical point of the analytical model and FE model are not located at exactly the same point. This is discussed further in section 5.

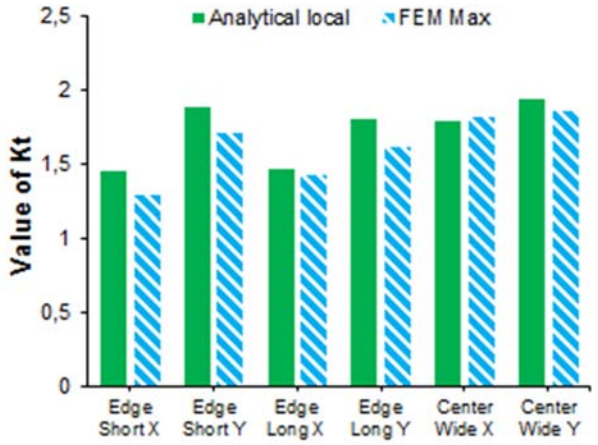

Figure 7. Maximum values of the stress concentration factor K_t in both x and y directions obtained with the analytical and FE models for the analysed topographies: *EdgeShort*, *EdgeLong* and *CentreWide*.

5. Discussion

This section discusses the differences found between the K_t results obtained by the FE model and the developed analytical model. In particular, a detailed analysis was carried out comparing the K_t results obtained for the *EdgeShort* surface. Since the points of both models did not match exactly, a linear regression was applied to the FE model data. Then, the results obtained with the FE model were extrapolated to the points used in the analytical model, and results were compared at the same points.

Figure 8.a shows the difference in the K_t calculated by the analytical and FE models, where the mean difference is 1.53%. Furthermore, a statistical analysis revealed a standard deviation σ=2.36%, which means that 99.7% (3σ) of the points have a difference lower than 7.1%. Therefore, from this statistical analysis it can be concluded that the difference between the models is low. However, the difference increased to

values higher than 10% in the deepest valley of the topography, as can be seen in Figure 8.a. These points also correspond to the critical values of the topography where the K_t is the highest (see Figure 8.b).

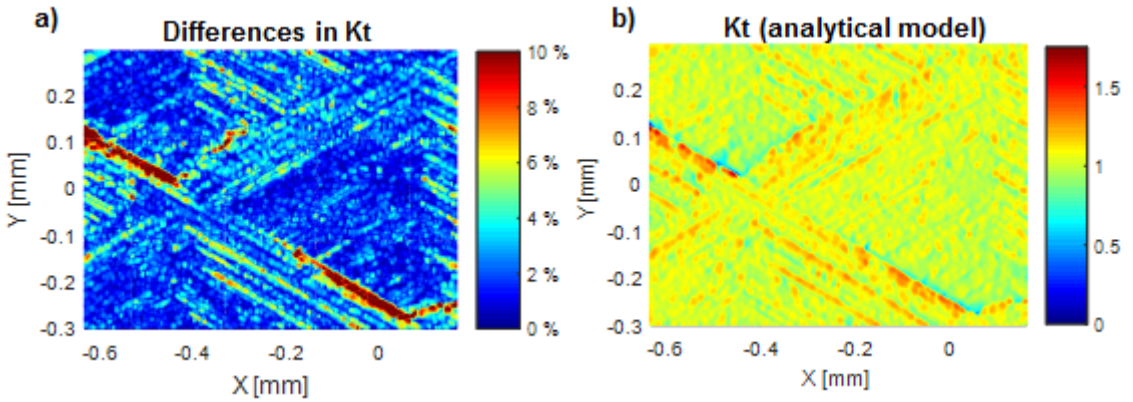

Figure 8. a) Distribution of the percentage difference in K_t value between FE and analytical in the surface *EdgeShort*, and b) K_t results for the analytical model.

The main cause for the differences in the calculation of K_t is possibly linked to the error in the fitting of the surface topography of both the analytical and FE models. For example, Ma *et al*. [45] established a criterion of a maximum relative error of 1% with respect to the original topography to validate the fitting of the surface topography. Figure 9 shows the error in the surface topography analysed in both the analytical and FE models with respect to the measured surface. For the analytical model (see Figure 9.a), the fitting of the surface is good, having a mean error of 0.07% and a maximum error of 0.3%. It should be noted that the error of the analytical topography, despite being small, is proportional to the surface topography, increasing in the peaks and valleys. In contrast, the FE model depicts a higher error randomly spread across the surface (see Figure 9.b). Even though the mean error is relatively small, with a value of 0.15%, the error increases considerably in the valleys of the topography, ranging from 0.41 to 2.18%. These results show that several points located in the deepest valley of the

FE model do not fulfil the criteria recommended by [45], and therefore may impact negatively on the calculation of the stress concentration factor. This topographic error observed in the FE model could have been generated during the transformation of the measured point cloud to a 3D geometry. Additionally, the error could have been caused by the mesh quality (size and type of elements). Nevertheless, reducing these errors would imply an increase of the computational cost of the FE model, since a higher amount of elements is required.

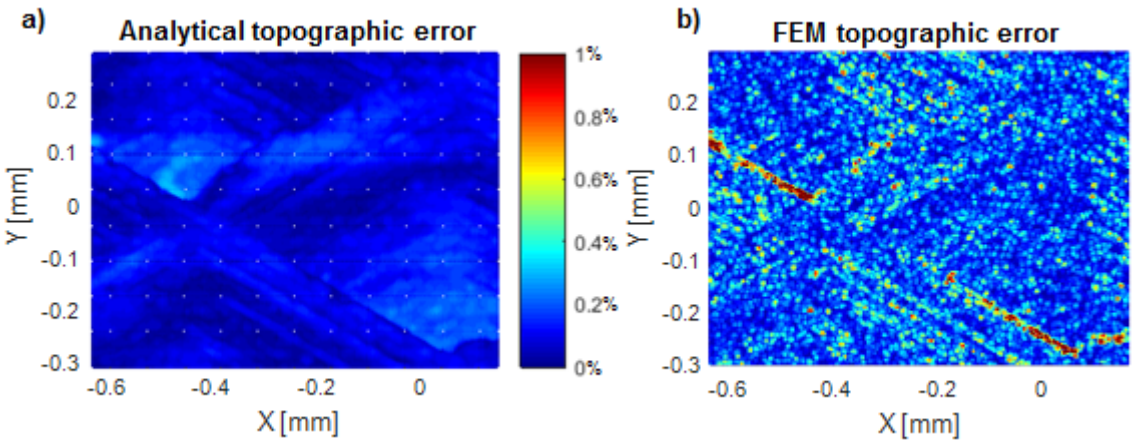

Figure 9. Error in the surface topography analysed in both a) the analytical, and b) FE models with respect to the measured surface *EdgeShort*

The error in the topography of the FE model and the difference in K_t between both models shows a similar trend. Comparing the differences in the topography between both models and the K_t difference, a linear relationship can be observed (see Figure 10). Even though there is a scatter of ±10%, the difference in the K_t is proportional to the topographic error. This implies that if both topographies were identical, the maximum difference in the value of K_t between FE and the analytical model would be between ±0.15.

Furthermore, the critical point of the analytical model, with a value of 1.67, has a topographic difference of 1.05% with respect to the FE model. As consequence of this topographic difference, the value of the K_t for the FE model is 1.24, with an error of 33.2%. Therefore, the main cause of the different critical points in both the FE and analytic models of some regions is due to the topographic differences between both models.

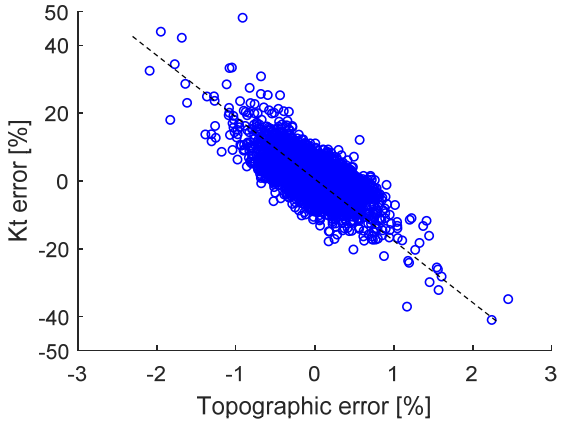

Figure 10. Effect of the topographic error on the error of K_t for all the analysed surfaces

One of the main advantages of the developed analytical model is the reduction of time for analysing the local effect of the topography on the stress concentration factor and the identification of critical points. Using the same computer, the FE models needed a computing time of 5.7-5.9 hours to calculate the stress concentration factor in each direction, while the analytical model required less than 1 min to perform the same calculus. Furthermore, the analytical model analysed surface regions that were 8 times greater than the reduced area used for the FE model. Therefore, the developed analytical model not only significantly reduces the computational cost (by 3,000 times), but it also enables the analysis of larger surfaces than the FE model.

6. Conclusions

The main conclusions of this work are:

- An analytical approach that enables us to calculate the stress concentration factor K_t of 3D surface topographies in different loading directions has been proposed and validated: the mean difference in the stress concentration factor K_t calculated by the analytical and FE models is 1.53%. Furthermore, the statistical analysis revealed a standard deviation σ=2.36%, which means that 99.7% (3σ) of the points have a difference lower than 7.1%.
- The proposed analytical approach accurately fits the surface topography measurements, with a mean deviation of 0.07% and a maximum deviation of 0.3%. The FE model shows a higher maximum deviation with respect to surface topography measurements, ranging from 0.41 to 2.18%. These deviations explain the highest differences between the K_t values of both models.
- Importantly, the developed analytical model reduces the computing time by 3,000 times compared to FE models, and enables the analysis of larger surfaces.

Acknowledgments

The authors thank the Basque Government for the financial support given to the project FRONTIERS (KK-2019/00077).

References

[1] R. Saoubi, J. C. Outeiro, H. Chandrasekaran, O. W. Dillon, and I. S. Jawahir, "A review of surface integrity in machining and its impact on functional performance and life of machined products", *Int. J. Sustain. Manuf.*, 2008, vol. 1, no. 1-2, pp. 203-236, doi: 10.1504/IJSM.2008.019234

[2] I.S. Jawahir, E. Brinksmeier, R. M'saoubi, D.K. Aspinwall, J.C. Outeiro, D. Meyer, ... & A.D. Jayal, ‘’Surface integrity in material removal processes: Recent advances’’, *CIRP annals*, 2011, vol. 60, no. 2, pp. 603-626, doi: 10.1016/j.cirp.2011.05.002

[3] D. Ulutan, and T. Ozel, "Machining induced surface integrity in titanium and nickel alloys: A review", *Int. J. Mach. Tools Manuf.*, 2011, vol. 51, no. 3, pp. 250-280, doi: 10.1016/j.ijmachtools.2010.11.003

[4] A. Thakur, and S. Gangopadhyay, "State-of-the-art in surface integrity in machining of nickel-based super alloys", *Int. J. Mach. Tools Manuf.*, 2016, vol. 100, pp. 25-54, doi: 10.1016/j.ijmachtools.2015.10.001

[5] D. Novovic, R. C. Dewes, D. K. Aspinwall, W. Voice, and P. Bowen, “The effect of machined topography and integrity on fatigue life”, *Int. J. Mach. Tools Manuf.*, 2004, vol. 44, no. 2–3, pp. 125–134, doi: 10.1016/j.ijmachtools.2003.10.018.

[6] S.A. McKelvey, A. Fatemi, "Surface finish effect on fatigue behavior of forged steel", *Int. J. Fatigue*, 2012, vol. *36, no.* 1, pp. 130-145, doi: 10.1016/j.ijfatigue.2011.08.008

[7] R. Aviles Gonzalez, "Análisis de fatiga en máquinas", 2005, Ediciones Paraninfo, SA.

[8] A.R.C. Sharman, D.K. Aspinwall, R.C. Dewes, D. Clifton, and P, "The effects of machined workpiece surface integrity on the fatigue life of γ-titanium aluminide", *Int. J. Mach. Tools Manuf*, 2001, vol. *41, no.* 11, pp. 1681-1685, doi: 10.1016/S0890-6955(01)00034-7

[9] T. Connolley, M.J. Starink, and P.A.S Reed, "Effect of broaching on high-temperature fatigue behavior in notched specimens of INCONEL 718", *Metall. Mater. Trans. A*, 2004, vol.35, no. 3, pp. 771-783, doi: 10.1007/s11661-004-0005-z

[10] D. Welling, "Results of surface integrity and fatigue study of wire-EDM compared to broaching and grinding for demanding jet engine components made of Inconel 718", *Procedia CIRP*, 2014, vol. 13, pp. 339-344, doi: 10.1016/j.procir.2014.04.057

[11] C. Herbert, D. A. Axinte, M. Hardy and P. Withers, "Influence of surface anomalies following hole making operations on the fatigue performance for a nickel based superalloy", *J. Manuf. Sci. Eng.*, 2014, vol. 136, no. 5, 051016, doi: 10.1115/1.4027619

[12] W.P. Koster, K. Field, L.J. Fritz, L.R. Gatto, J.F. Kahles, "Surface integrity of machined structural components", No. 970-11700, *Metcut Research Associates Inc Cincinnati Oh*, 1970

[13] F. Hashimoto, Y.B. Guo, and A.W. Warren, " Surface integrity difference between hard turned and ground surfaces and its impact on fatigue life. *CIRP annals*, 2006, vol. 55, no. 1, pp. 81-84, doi: 10.1016/S0007-8506(07)60371-0

[14] S. Smith, S.N Melkote, E. Lara-Curzio, T.R. Watkins, L. Allard, & L. Riester, "Effect of surface integrity of hard turned AISI 52100 steel on fatigue performance", *Mater. Sci. Eng. A*, 2007, vol. 459, no. 1-2, pp. 337-346, doi: 10.1016/j.msea.2007.01.011

[15] A. Javidi, U. Rieger, and W. Eichlseder, "The effect of machining on the surface integrity and fatigue life", *Int. J. Fatigue*, 2008, vol. 30, no. 10-11, pp. 2050-2055, doi: 10.1016/j.ijfatigue.2008.01.005

[16] S.L. Soo, M.T. Antar, D.K. Aspinwall,C. Sage, M. Cuttell, R. Perez, and A.J. Winn, "The effect of wire electrical discharge machining on the fatigue life of Ti-6Al-2Sn-4Zr-6Mo aerospace alloy", *Procedia CIRP*, 2013, vol. 6, pp. 215-219, doi: 10.1016/j.procir.2013.03.043

[17] R. Galatolo and D. Fanteria, D, "Influence of turning parameters on the high-temperature fatigue performance of Inconel 718 superalloy", *Fatigue Fract. Eng. Mater. Struct.* , 2017, vol. 40, no. 12, pp. 2019-2031, doi: 10.1111/ffe.12623

[18] Y. Hua, and Z. Liu, "Experimental Investigation of Principal Residual Stress and Fatigue Performance for Turned Nickel based Superalloy Inconel 718", *Mater.*, 2018, vol. 11, no. 6, pp. 879, doi 10.3390/ma11060879

[19] A. Pramanik, A.R. Dixit, S. Chattopadhyaya, M.S. Uddin, Y. Dong, A.K. Basak, & G. Littlefair. "Fatigue life of machined components", *Adv. Manuf*, 2017, vol. 5, no. 1, pp. 59-76, doi: DOI 10.1007/s40436-016-0168-z

[20] S. Jeelani, and M. Musial, "Effect of cutting speed and tool rake angle on the fatigue life of 2024-T351 aluminium alloy", *Int. J. Fatigue*, 1984, vol. 6, no. 3, pp. 169-172, doi: 10.1016/0142-1123(84)90034-3

[21] Q. Huang and J.X. Ren, "Surface integrity and its effects on the fatigue life of the nickel-based superalloy GH33A", *Int. J. Fatigue*, 1991, vol. 13, no. 4, pp. 322-326, doi: 10.1016/0142-1123(91)90359-7

[22] S. K. Ås, B. Skallerud, B. W. Tveiten, and B. Holme, “Fatigue life prediction of machined components using finite element analysis of surface topography”, *Int. J. Fatigue*, 2005, vol. 27, no. 10–12, pp. 1590–1596, doi: 10.1016/j.ijfatigue.2005.07.031.

[23] M. Suraratchai, J. Limido, C. Mabru, and R. Chieragatti, “Modelling the influence of machined surface roughness on the fatigue life of aluminium alloy”, *Int. J. Fatigue*, 2008, vol. 30, no. 12, pp. 2119-2126, doi: 10.1016/j.ijfatigue.2008.06.003

[24] F. Abroug, E. Pessard, G. Germain, F. Morel, and E. Chové, “The effect of machining defects on the fatigue behaviour of the Al7050 alloy”, 2016, *Open Repository ENSAM*, http://hdl.handle.net/10985/11342

[25] A. Thompson, N. Senin, C. Giusca, and R. Leach, "Topography of selectively laser melted surfaces: a comparison of different measurement methods", *CIRP Annals*, 2017, vol. 66, no. 1, pp. 543-546, doi: 10.1016/j.cirp.2017.04.075

[26] A. Zabala, L. Blunt, W. Tato, A. Aginagalde, X. Gomez, and I. Llavori, "The use of areal surface topography characterisation in relation to fatigue performance", *In MATEC Web of Conferences*, 2018, vol. 165, pp. 14013, EDP Sciences, doi: 10.1051/matecconf/201816514013

[27] D. Yang, Z. Liu, X. Xiao, and F. Xie, "The effects of machining-induced surface topography on fatigue performance of titanium alloy Ti-6Al-4V", *Procedia CIRP*, 2018, vol. 71, pp. 27-30, doi: 10.1016/j.procir.2018.05.015

[28] M. Vulliez, M. Gleason, A. Souto-Lebel, Y. Quinsat, C. Lartigue, S. Kordel, ... and C. Brown, "Multi-scale curvature analysis and correlations with the fatigue limit on steel surfaces after milling", *Procedia CIRP*, 2014, vol. 13, 308 – 313, doi: 10.1016/j.procir.2014.04.052

[29] Q. Zeng, Y. Qin, W. Chang, and X. Luo, "Correlating and evaluating the functionality-related properties with surface texture parameters and specific characteristics of machined components", *Int. J. Mech. Sci.*, 2018, vol. 149, pp. 62-72, doi: 10.1016/j.ijmecsci.2018.09.044

[30] M.R. Bayoumi and A.K. Abdellatif, "Effect of surface finish on fatigue strength", *Eng. Fract. Mech.*, 1995, vol. 51, no. 5, pp. 861-870, doi: 10.1016/0013-7944(94)00297-U

[31] Peterson RE. Stress concentration factors. New York: John Wiley and Sons 1974.

[32] H. Neuber, *Kerbspannungslehre*. Springer Berlin Heidelberg, 1958.

[33] D. Arola and M. Ramulu, “An Examination of the Effects from Surface Texture on the Strength of Fiber Reinforced Plastics”, *J. Compos. Mater.*, 1999, vol. 33, no. 2, pp. 102–123, doi: 10.1177/002199839903300201.

[34] D. Arola and C.L. Williams, "Estimating the fatigue stress concentration factor of machined surfaces", *Int. J. Fatigue*, 2002, vol. *24*, no. 9, pp.923-930, doi: 10.1016/S0142-1123(02)00012-9

[35] H. Medina and B. Hinderliter, “The stress concentration factor for slightly roughened random surfaces: Analytical solution”, *Int. J. Solids Struct.*, 2014, vol. 51, no. 10, pp. 2012–2018, doi: 10.1016/j.ijsolstr.2014.02.011.

[36] W. Huang, J. Zhao, A. Xing, G. Wang, and H. Tao, “Influence of tool path strategies on fatigue performance of high-speed ball-end-milled AISI H13 steel,” *Int. J. Adv. Manuf. Technol.*, 2018, vol. 94, no. 1–4, pp. 371–380, doi: 10.1007/s00170-017-0841-9.

[37] Souto-Lebel, A., 2014. Rôle de l’intégrité de surface dans la tenue en fatigue d’un acier bainitique après fraisage de finition, PhD Thesis, Cachan: ENS Cachan.

[38] S. K. Ås, B. Skallerud, and B. W. Tveiten, “Surface roughness characterization for fatigue life predictions using finite element analysis,” *Int. J. Fatigue*, 2008, vol. 30, no. 12, pp. 2200–2209, doi: 10.1016/j.ijfatigue.2008.05.020.

[39] F. Abroug, E. Pessard, G. Germain, and F. Morel, “A probabilistic approach to study the effect of machined surface states on HCF behavior of a AA7050 alloy”, 2018, *Int. J. Fatigue*, vol. 116, pp. 473–489, doi:

10.1016/j.ijfatigue.2018.06.048.

[40] G.W Li, J.Y Tang, W. Zhou, and L. Li, “Fatigue life prediction of workpiece with 3D rough surface topography based on surface reconstruction technology,” *J. Cent. South Univ.*, 2018, vol. 25, no. 9, pp. 2069–2075, doi: 10.1007/s11771-018-3896-3.

[41] D.T Ardi, Y: G Li, K. H. K. Chan, L. Blunt and M.R. Bache, "Surface topography and the impact on fatigue performance", 2015, *Surf. Topogr.: Metrol. Prop.*, vol. *3,* no. 1, pp 015007, doi: 10.1088/2051-672X/3/1/015007

[42] H. Medina, “A stress-concentration-formula generating equation for arbitrary shallow surfaces,” *Int. J. Solids Struct.*, 2015, vol. 69–70, pp. 86–93, doi: 10.1016/j.ijsolstr.2015.06.006.

[43] H. Gao "A boundary perturbation analysis for elastic inclusions and interfaces", *Int. J. Solids Struct.*, 1991, vol. *28, no.* 6, pp. 703-725, doi: 10.1016/0020-7683(91)90151-5

[44] Z. Cheng, R. Liao, and W. Lu, “Surface stress concentration factor via Fourier representation and its application for machined surfaces”, *Int. J. Solids Struct.*, 2017, vol. 113–114, pp. 108–117, doi: 10.1016/j.ijsolstr.2017.01.023.

[45] L. Ma, G. Xu, G. Wang, and M. Zhao, “A new method for evaluating the influences of surface topography on fatigue propriety of the random machined surfaces”, *MATEC Web of Conferences*, 2018, vol. 165, doi: 10.1051/matecconf/201816522028.

[46] C. Kantzos, J. Lao, and A. Rollett, “Design of an interpretable Convolutional Neural Network for stress concentration prediction in rough surfaces”, *Mater. Charact.*, 2019, vol. 158, Dec. 2019, doi: 10.1016/j.matchar.2019.109961.

[47] R. A. Lebensohn, A. K. Kanjarla, and P. Eisenlohr, “An elasto-viscoplastic formulation based on fast Fourier transforms for the prediction of micromechanical fields in polycrystalline materials”, *Int. J. Plast.*, 2012, vol. 32–33, pp. 59–69, doi: 10.1016/j.ijplas.2011.12.005.

[48] Y. Aono and H. Noguchi, “Fatigue limit reliability of axisymmetric complex surface”, *Int. J. Fract.*, 2005, vol. 131, no. 1, pp. 59–78, doi: 10.1007/s10704-004-3638-4.

[49] C.A. Brown, H.N. Hansen, X.J. Jiang, F. Blateyron, J. Berglund, N. Senin, … & W.J. Stemp, ‘’Multiscale analyses and characterizations of surface topographies’’, *CIRP annals*, 2018, vol.67, no. 2, pp. 839-862, doi: 10.1016/j.cirp.2018.06.001

[50] J.W. Cooley, P. Lewis, P., and P. Welch, ‘’Application of the fast Fourier transform to computation of Fourier integrals, Fourier series, and convolution integrals’’, *IEEE Trans. Audio Electroacous*., 1967, vol. 15, no. 2, pp. 79-84, doi: 10.1109/TAU.1967.1161904

[51] J.P. Allebach, N.C. Gallagher, and B. Liu, ‘’Aliasing error in digital holography’’, *Appl. Opt.*, 1976, vol. 15, no. 9, pp. 2183-2188, doi: 10.1364/AO.15.002183